frontiers | Frontiers in Chemistry

TYPE Original Research
PUBLISHED 14 November 2022
DOI 10.3389/fchem.2022.1066958

Check for updates

OPEN ACCESS

EDITED BY
Min Wang,
China University of Petroleum (East China), China

REVIEWED BY
Hafiz Muhammad Adeel Sharif,
Dongguan University of Technology, China
Muhammad Arsalan,
Qatar University, Qatar

*CORRESPONDENCE
Hai-Jun Zhang,
zhanghaijun@tongji.edu.cn
Zhang Jun,
junzhang@tongji.edu.cn

SPECIALTY SECTION
This article was submitted to Electrochemistry, a section of the journal *Frontiers in Chemistry*

RECEIVED 11 October 2022
ACCEPTED 26 October 2022
PUBLISHED 14 November 2022

CITATION
Khan AR, Zhang H-J, Jun Z, Eldin SM, Alsaiari NS and Katubi KM (2022), Electrochemical corrosion resistance of aluminum alloy 6101 with cerium-based coatings in an alkaline environment. *Front. Chem.* 10:1066958. doi: 10.3389/fchem.2022.1066958

COPYRIGHT
© 2022 Khan, Zhang, Jun, Eldin, Alsaiari and Katubi. This is an open-access article distributed under the terms of the Creative Commons Attribution License (CC BY). The use, distribution or reproduction in other forums is permitted, provided the original author(s) and the copyright owner(s) are credited and that the original publication in this journal is cited, in accordance with accepted academic practice. No use, distribution or reproduction is permitted which does not comply with these terms.

Electrochemical corrosion resistance of aluminum alloy 6101 with cerium-based coatings in an alkaline environment

Ahsan Riaz Khan[1,2,3], Hai-Jun Zhang[1,2]*, Zhang Jun[4,5]*, Sayed M Eldin[6], Norah Saleem Alsaiari[7] and Khadijah Mohammedsaleh Katubi[7]

[1]Department of Interventional and Vascular Surgery, Shanghai Tenth People's Hospital, Tongji University School of Medicine, Shanghai, China, [2]National United Engineering Laboratory for Biomedical Material Modification, Branden Industrial Park, Qihe Economic & Development Zone, Dezhou, Shandong, China, [3]Department of Chemical Engineering, Northwest University, Xi'an, China, [4]Research Center for Translational Medicine, Shanghai East Hospital, School of Medicine, Tongji University, Shanghai, China, [5]Shanghai Institute of Stem Cell Research and Clinical Translation, Shanghai, China, [6]Center of Research, Faculty of Engineering, Future University in Egypt, New Cairo, Egypt, [7]Department of Chemistry, College of Science, Princess Nourah bint Abdulrahman University, Riyadh, Saudi Arabia

Chromium-free materials as eco-friendly coatings with higher corrosion resistance are crucial in various industrial processes. Herein, we report the deposition of cerium-based conversion, a chromium-free, eco-friendly chemical conversion coating for aluminum alloy 6101, by the dip coating method. Immersion in cerium salt precursors assisted with hydrogen peroxide was performed for the deposition of cerium-based conversion coatings on aluminum alloy 6101 at different bathing temperatures. The electrochemical corrosion behavior was assessed in an alkaline solution of sodium hydroxide (pH 11), including mass loss measurements, free corrosion risk, polarization, and electrochemical impedance spectroscopy. X-ray diffraction and photoelectron spectroscopy analysis showed that the coatings were composed of Ce (III) and Ce (IV) oxides. Surface modifications and surface degradation of the coating and substrate after immersion in corrosive media were analyzed by scanning electron microscopy. Additionally, energy dispersive scanning analysis demonstrated the elemental composition before and after corrosion of the cerium salt conversion-based coating. The results demonstrated that selectively deposited cerium-based conversion coatings improved the corrosion resistance by up to 96% in a strong corrosive alkaline media.

KEYWORDS

conversion, cerium, electrochemistry, coating, corrosion

1 Introduction

Conversion coatings are used to protect organic coatings from corrosion and to improve their adhesive properties. Conversion coatings have been used in industry for over a century. Conversion coating is a process that changes the surface metal oxide to a coating with different properties that integrates metal cations from the base metal (Li et al., 2022; Campestrini et al., 2004; Andreeva et al., 2016). The need to include cations originating from the substrate metal is removed by the broader definition. The industrial use of these coatings requires efficient processes (Castano et al., 2015; Zaman et al., 2021; Khan et al., 2022a). In recent years, the research community has adopted the phrase to represent any base-level rust coverage but does not always adhere to the exact processing requirements dictated by industrial processes, a fact that must be considered in the literature. Thus, the methods presented in the literature may not meet the requirements for industrial applications (Chen et al., 2021; Chauhan et al., 2022).

Anticorrosive treatments such as chromate conversion coatings (CCCs) have been employed for aluminum, tin, zinc, and steel. CCCs, primer, and paint systems are commonly used to protect aluminum alloy components from corrosion, in which the film coating plays a unique role in the defense mechanism (Zaman et al., 2022a; Sharif et al., 2023). However, despite the feature and benefits, due to the hazardous and carcinogenic nature of CCCs chemical dip treatment techniques when mixed with sodium dichromate solutions, there is an urgent need for updated processes (Chen et al., 2015; Eslami et al., 2017). Despite extensive investigation, no appropriate substitute treatment has yet been reported. The environmentally friendly substitutes to CCCs that have been examined as possible replacements include anodizing, rare-earth coatings, and pigments (Fahrenholtz et al., 2002; Harvey, 2013).

Due to their low costs, high strength-to-weight ratios, and corrosive resistance, aluminum alloys are widely used in various industries including automotive, aerospace, architecture, and desalination sectors (Khan et al., 2022c; Sharif et al., 2022). However, the different microstructures of aluminum alloys are vulnerable to local corrosion due to interactions between chloride ions (adsorbed on the substrate surface) and aluminum oxide layers, which reduces the metal thickness (Hughes et al., 2004; Khan et al., 2022c).

Rare-earth elements such as Nd, Pr, La, and Ce (Hasannejad et al., 2008; Zaman et al., 2022b) provide extraordinary resistance to localized corrosion by forming insoluble hydroxide/oxide layers. These elements are not considered hazardous due to their low toxicity. Therefore, coatings containing Ce and other rare-earth elements have been suggested as prospective substitutes for chromate-based preparations in metallic finish processes for aluminum alloys (Hughes et al., 2004; Joshi et al., 2012).

Hinton et al. (2003) presented one of the most researched systems, containing different rare-earth salts consisting of ions that produce unsolvable hydroxides with extraordinary resistance to localized corrosion (Kamde et al., 2021; Khast et al., 2022). The chemical reduction of (H_2O_2) causes the rapid deposition of Ce at cathodic sites in an aqueous media comprehending Ce (III) ions with H_2O_2 (Kulinich et al., 2007). The formation of hydroxyl ions in the cathode leads to a local increase in pH on the alloy surface, which promotes the formation of precipitates or/soluble ionic complexes in $Ce(OH)_3$ such as $Ce(OH)_2^{2+}$.

Generally, Ce (III) is thought to be oxidized to Ce (IV) in solution because it contains oxidizing agents (Kulinich et al., 2007; Kiyota et al., 2011). Since the Ksp of $Ce(OH)_4$ is 4.010^{-51}, the Ksp of Ce $(OH)_3$ is significantly smaller (1.510^{-20}). Ce (IV) deposition occurs at a lower pH compared to $Ce(OH)_3$.

The present study evaluated the corrosion characteristics of Ce-conversion coatings on aluminum alloy 6101 based on the use of chloride and nitrate ions from Ce sources, conversion solution pH, different temperatures, and H_2O_2. The corrosive characteristics of alloy 6101 treated with the Ce-conversion coating, have not been thoroughly reported previously. Corrosion potential, polarization curve, XPS, and electrochemical impedance spectroscopy (EIS) have been used to investigate corrosion behavior supported by weight loss tests.

2 Material and methods

2.1 Materials

Specimens of commercially available aluminum alloy 6101 with nominal composition percents by weight of Si (0.3%–0.7%), Fe (≤0.50%), Cu (≤0.10%), Mn (≤0.03%), Mg (0.35%–0.8%), and Cr (≤0.03%) measuring 40 × 20 × 5 mm were tested. Analytical-grade chemicals with 99.99% purity, including cerium nitrate hexahydrate ($Ce(NO_3)_3.6H_2O$) and hydrogen peroxide (H_2O_2), were obtained from the Tianjin Damao chemical reagent factory. Similarly, ethanol (CH_3CH_2OH), sodium hydroxide (NaOH), and nitric acid (HNO_3) with 99% purities were obtained from Tianjin Fuyu Fine Chemicals Co., Ltd. (Table 1). Moreover, electro-coated and waterproof gelatin and carbide paper were obtained from Fuchen (Tianjin) Chemical Reagent Co., Ltd., and Matador Co., Ltd., respectively.

2.1.1 Sample and surface preparation

Before the conversion coating treatment, the samples were mechanically polished to 1,200 g before being processed with silicon carbide (SiC) paper to enhance the surface modification for better adhesion of the Ce coating. To prevent surface defects, the following chemical pretreatments including an ethanol rinse and an acetone ultrasonic rinse for 10 min were performed at ambient temperature. Additionally, a 30 s

TABLE 1 Chemical compositions of Ce-based conversion coatings.

Conversion coatings	Concentration (mol L^{-1})	Composition of coating	Chemical formula
Coating	0.02 + 1 (30vol%)	Cerium nitrate hexahydrate + hydrogen peroxide	Ce $(NO_3)_3.6H_2O + H_2O_2$

cleaning, removal of dust particles present on the surface of the substrate with nitric acid (HNO_3) solution, and etching in an alkaline solution of 1M sodium hydroxide (NaOH) were performed. After cleaning the surface of the aluminum alloy 6101 with acetone, the samples were rinsed with deionized water and stored in a desiccator for further experimentation to avoid surface defects and ensure the consistency of the surface hydroxides and oxides.

2.2 Coating formation and deposition

2.2.1 Potential effects of temperature and heat on coating formation

The solution color changes are shown in Figure 1. Upon the addition of H_2O_2, the solution gradually turned golden yellow after boiling to 50°C. Continuous heating of the mixture at 70°C resulted in the removal of the dark orange suspended particles. This change may be due to the reaction that occurs after the solution.

$$H_2O_2 + 2_{e^-} \rightarrow 2OH^- \quad (1)$$

$$4Ce^{3+} + O_2 + 4OH^- + 2H_2O \rightarrow 4Ce(OH)_2^{2+} \quad (2)$$

$$Ce(OH)_2^{2+} + 2OH^- \rightarrow Ce(OH)_4 \rightarrow CeO_2 + 2H_2O \quad (3)$$

A high-temperature aqueous media along with a maximum consumption of H_2O_2 increases reaction kinetics, leading to the rapid utilization of coated-forming species in the cerium-based conversion media before the sample treatment. As the reduction of the number of reacting species also reduces the quantity of Ce coating the surface during the conversion coating treatment, the Ce–H_2O_2 transformation coating solution was first prepared at ambient temperature (25°C). The conversion coating was then applied in a solution continuously heated at 50°C–70°C (T70°C, 5°C/min heating rate for 8 min to stop the early fuming evaporation of the coating-forming species). Figure 2 shows the surface of the samples during coating at 50°C and 70°C. Under these temperature conditions, golden yellow surfaces formed, suggesting that cerium coatings formed under these conditions (Hasannejad et al., 2008; Chen et al., 2021).

2.2.2 Coating deposition

Different aqueous solution treatment temperatures were utilized as the sources of Ce for the chemical conversion

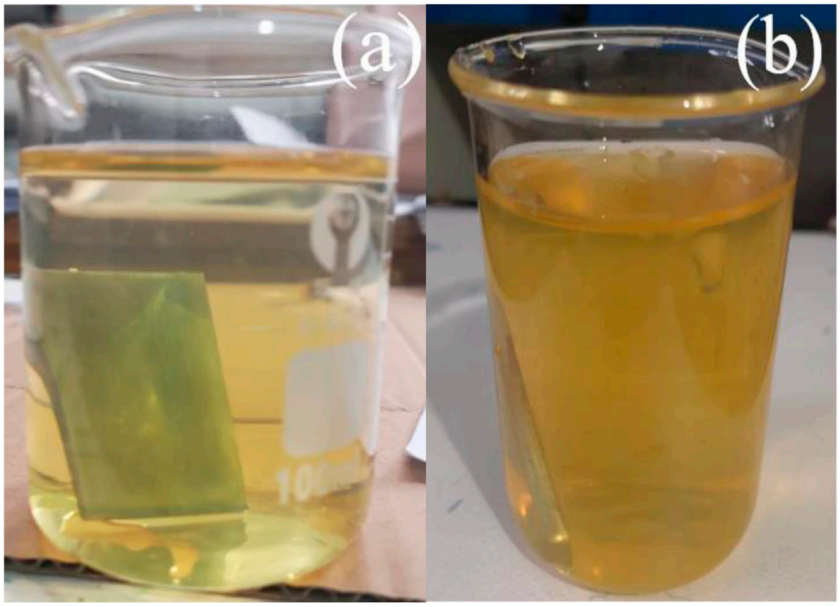

FIGURE 1
Two different colors of cerium conversion coatings at **(A)** 50°C and **(B)** 70°C temperature baths.

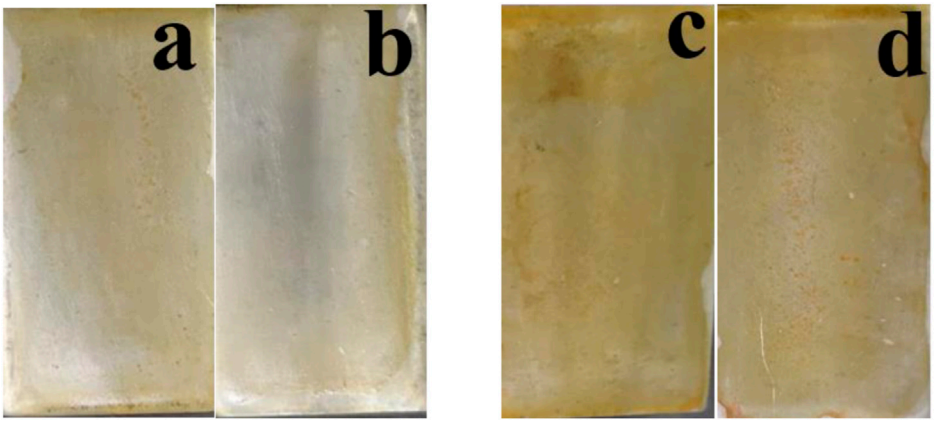

FIGURE 2
Coating deposition after the preparation of cerium conversion coatings. **(A,B)** At 50°C and **(C,D)** 70°C.

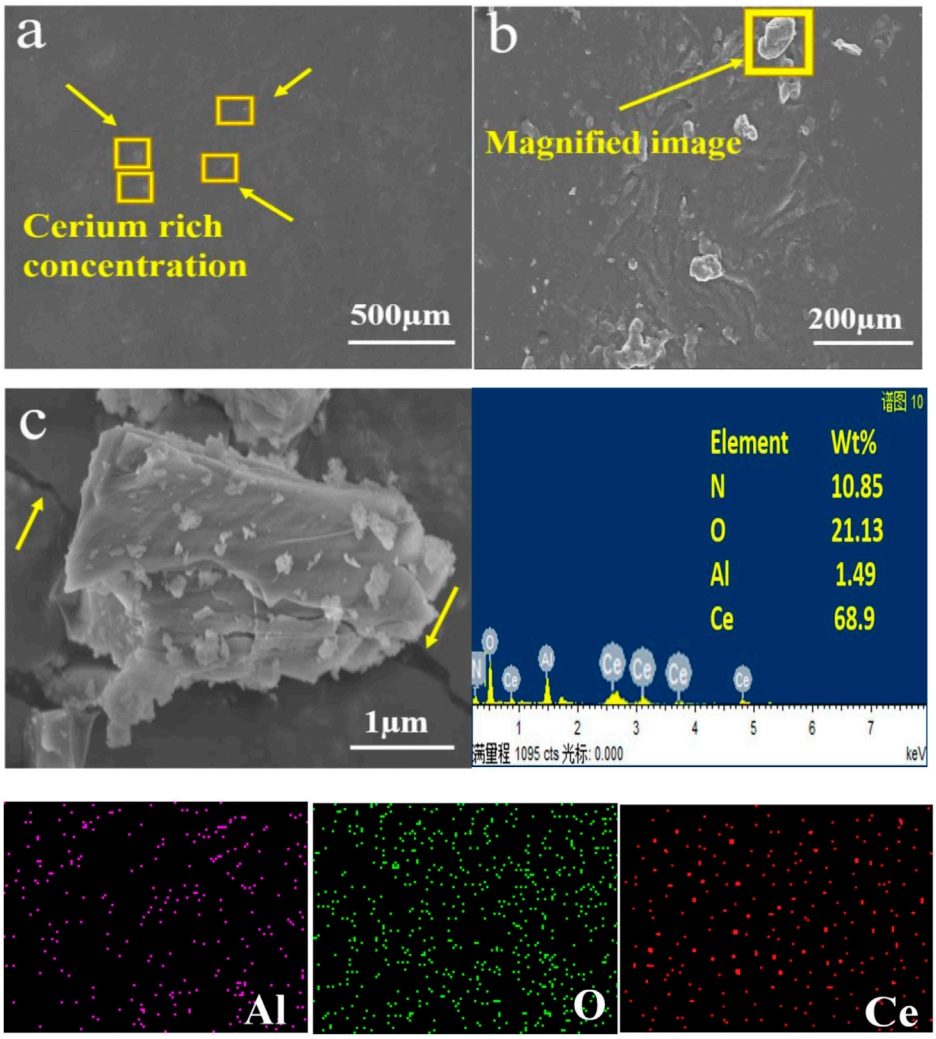

FIGURE 3
SEM images of the Ce-based conversion coating on the Al alloy 6101 before the corrosion test showing **(A)** homogenous coating on the substrate and **(B)** enrichment of the coating, as well as **(C)** EDS elemental analysis.

coating. Solutions were produced at 50°C and 70°C, respectively, carefully agitated for 10 and 20 min, and utilized immediately after the addition of H_2O_2. A thermopotentiometer was used to measure the pH of the liquids (pH=5.2), which was adjusted by adding gelatin. Before the electrochemical experiments, the treated specimens were washed for 24 h at ambient temperature and dried. The chemical pre-treatment, coating temperature, reagent concentrations, and immersion time were pre-optimized in the laboratory. Single coatings are very thin and cannot resist the harsh corrosive environment for long; therefore, four rounds of coating were applied to the substrate to attain the desired coating thickness for better results (Figure 3). An average coating thickness of approximately 20 ± 5 μm was measured.

2.3 Surface morphology

The coating surfaces were observed by scanning electron microscopy (SEM). Energy-dispersion X-ray spectroscopy (EDS) and X-ray photoelectron spectroscopy (XPS) are used to analyze coating compositions (Khan et al., 2022a). The samples were PVD-plated with a Pt film before SEM and EDS analyses. X-ray diffraction (XRD) based on the 2500VB2+PC diffractometers in China was used to investigate the composition of the coatings using concentrated filtered Cu K radiation.

2.4 Corrosion test measurements

To characterize the corrosion resistance of the cerium-based conversion coatings, electrochemical and effective weight loss corrosion tests were performed. A PARSTAT 2273 potentiate electrochemical workstation was used for the electrochemical test measurements. The electrochemical station consists of a three-electrode (250 ml) cell, a working electrode (coated aluminum alloy), a platinum spade, and a saturated calomel electrode (SCE) with an auxiliary capillary as the reference electrode. The effective weight loss corrosion test was carried out by immersing the aluminum test sample in a basic solution of NaOH at pH 11 for 72 h, with weight readings every 12 h. The basic NaOH solution (pH 11) was used due to the severe aluminum alloy corrosion in alkaline conditions (Li et al., 2013; Mohammadloo et al., 2014).

If the initial weight is W_0, after corrosion, the weight is defined as W_1; thus, the apparent corrosion rate due to weight loss is

$$V = \frac{W_0 - W_1}{A \times t} \tag{4}$$

Where V is the apparent corrosion rate due to corrosion in mass change g/(m^2·h), W_0 is the initial weight, W_1 is the final weight, A is the corrosion area, and t is the corrosion time.

An alternate form of Eq. 5 in depth is

$$V_d = \frac{8.75V}{\rho} \tag{5}$$

Where V_d is the annual corrosion rate (mm/a) and ρ is the density of metal (g/cm^3).

The protection efficiency can be calculated by following equation,

$$\eta\% = [(V_{dBlank} - V_{dCoated})/ V_{dBlank}] \times 100 \tag{6}$$

where C_{dBlank} and $C_{dCoated}$ represent the corrosion rates of the blank and coated metals, respectively.

3 Results and discussion

3.1 Mass loss corrosion test

After cleaning and drying, the effective weight losses of the bare and coated samples were measured to assess the apparent corrosion rates. The weight loss was measured by immersing the specimens in an alkaline solution of NaOH with a pH of 11 and measuring the weight change every 12 h. The alkaline solution was changed daily to maintain a constant pH. The specimens were then washed with deionized water before drying at 60°C for 20 min.

The samples with a cerium-based coating showed decreasing trends in weight loss and corrosion rates. Table 2 shows the mass loss and potentiodynamic polarization measurements at pH 11 for the coated and blank aluminum samples at various cerium salt concentrations. The mass loss showed an inhibition efficiency of 96.59% in the alkaline solution of NaOH with a coating efficiency of 52%. The inhibitor layer formed on the metal substrate protected the substrate surface from the corrosive media.

TABLE 2 Comparison of effective weight loss for Al alloy 6101 coated and blank samples in the NaOH corrosion solution (pH 11).

Serial no.	pH	V/g·m^{-2}·h^{-1}	Std. Dev., σ	V_d/mm·a^{-1}	η_w%
24 h	11	0.90	0.24	0.016	96.59
48 h	11	1.06	0.18	0.020	92.77
72 h	11	6.68	0.22	0.017	52.91
Blank	11	14.3	-	0.265	-

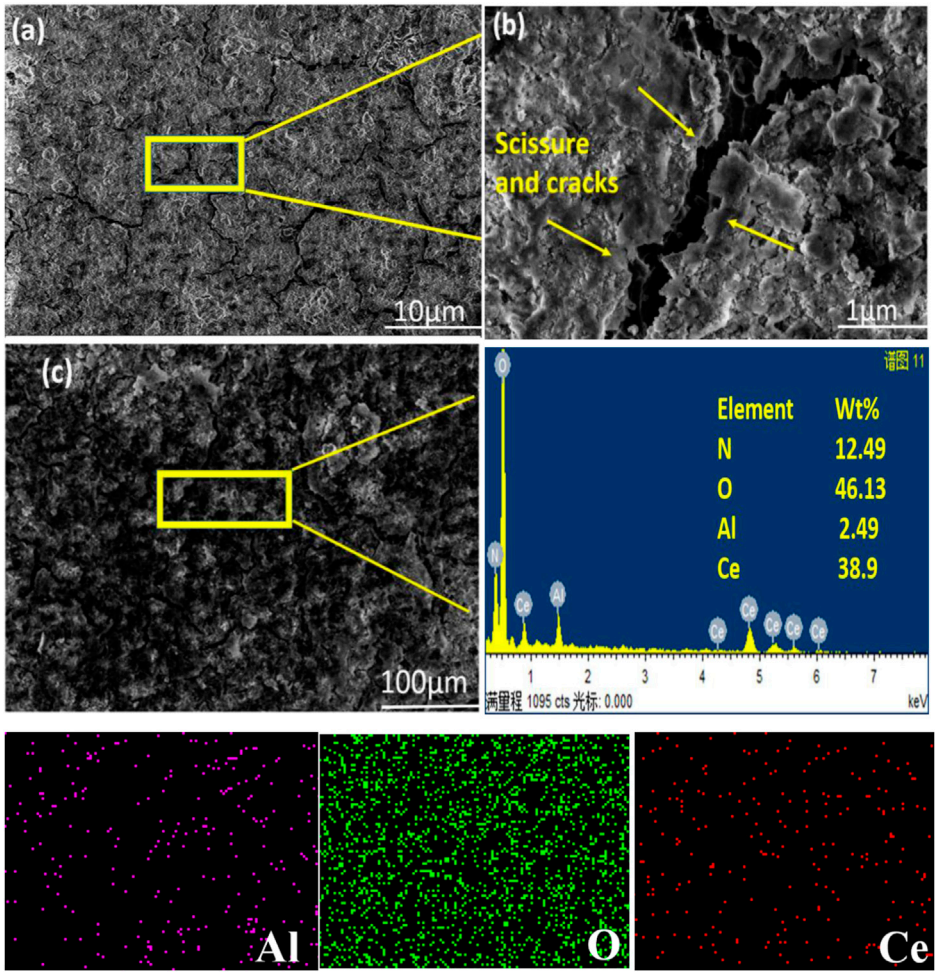

FIGURE 4
SEM images of the coating after 21 days of immersion in an alkaline NaOH solution. **(A)** showing cracks, **(B)** magnified mage, and **(C)** EDS of the elemental concentration.

3.2 Surface morphology

SEM images were obtained of Al alloy 6101 with cerium oxide coating. Although the coating was stable and smooth, cracks were noted. Numerous researchers have cited the appearance of scissures and cracks typical of layers made from hydroxide due to the dehydration of cerium conversion coatings (Pardo et al., 2007; Paussa et al., 2012). An SEM image of the coating is shown in Figure 4, which comprises laminated layers and has a very fine thickness on the substrate surface. Numerous columnar formations were observed in each layer. Investigation of the conformation of the cerium-based eco-friendly coatings thru EDS and the elemental contents (wt%) showed N (12.49%), O (46.13%), Al (2.49%), Ce (38.09%). Therefore, the-dip coating of aluminum alloy 6101 cerium oxide-based mostly consisted of Ce, O, Al, and N elements (Sainis and Zanella, 2022).

3.3 XPS analysis

XPS was used to assess the bonding of the elements in the coating. XPS analysis of the cerium-based coatings in Figure 5A showed the wide spectrum of Ce deposited on the coating surface. Ce, O, and C comprised most of the coating's floor composition. The absence of Al peaks in the matrix showed that the coated surface was devoid of

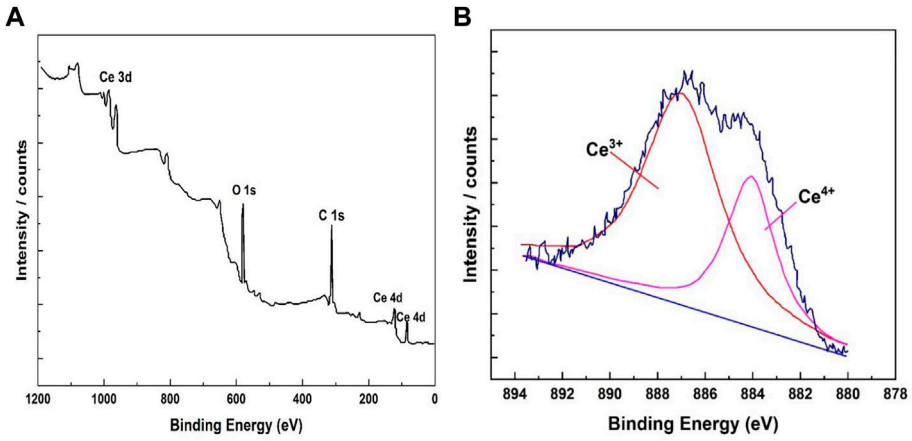

FIGURE 5
XPS band ranges of the cerium coatings. **(A)** Examination band spectrum. **(B)** Cerium-based conversion coating peaks.

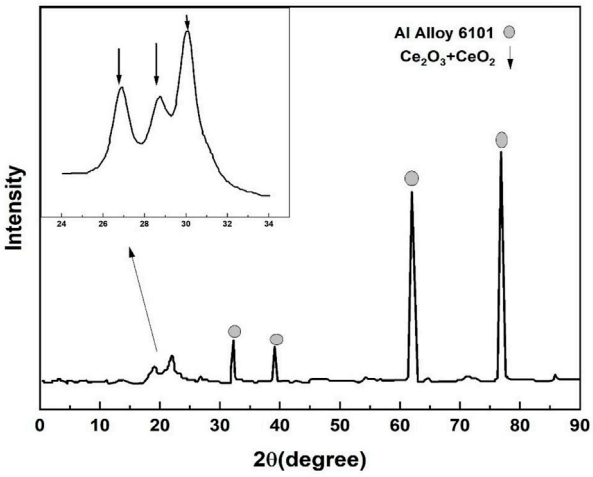

FIGURE 6
XRD peaks of the cerium coatings.

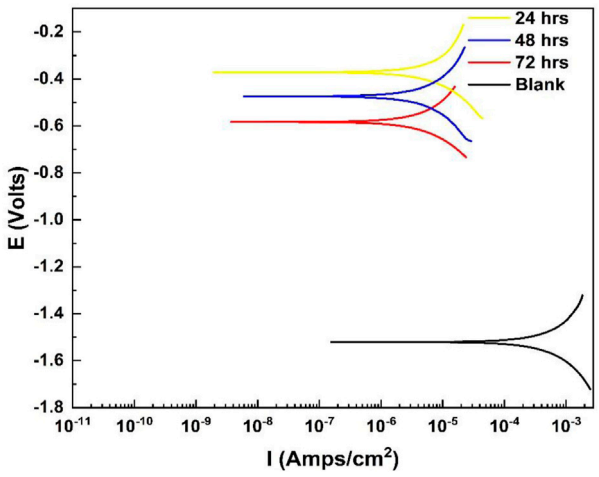

FIGURE 7
Tafel curves of the coated and bare Al alloy 6101 samples in the 0.001 M NaOH solution (pH 11).

aluminum or its compounds. The overlapping Ce (IV) and Ce showed as the rare Ce peak between 878 and 892 eV (III). Similarly, Figure 5B shows the deconvolution of the Ce peak. The peak zone proportion of Ce (III)/Ce (IV), 0.45, was used to compute the comparative contents of cerium (III) and cerium (IV).

3.4 XRD characterization

The XRD patterns of the dip-coated cerium conversion coatings are shown in Figure 6. The deflection peaks at 2θ = 25.417° and 2 = 28.445° could be related to planes (101) and (012) for Ce_2O_3 according to XRD. The small specific shoulder peak on the leftward side of the (002) peak may be due to the (111) replication of CeO_2. The reason behind earlier reported cerium oxide coatings were primarily composed of Ce (IV) species, which may be related to the use of H_2O_2 in the conducting solution (Scholes et al., 2006).

The dip coating has been hypothesized to provide extra dissolved oxygen even without H_2O_2 in the coating solution. Throughout the dipping process, the coating species frequently settled in layers on the surface of the coated specimens (Tang et al., 2011), which may have caused more oxygen to dissolve in the electrolyte solution. Dissolved oxygen has less oxidizing power compared to H_2O_2. The oxidation of Ce (III) to Ce (IV) is difficult in single or spray coating processes, which

TABLE 3 Comparison of electrochemical measurements for coated and blank Al alloy 6101 samples in the corrosion solution (pH 11).

Sample	pH	E_0/V	I_0/Amp/cm^2 (E)	Ba/mV	Std. Dev., σ	Bc/mV	Corrosion rate (mm/a)	ηp,%
24 h	11	−0.624	1.254^{-5}	28.17	1.80	−236.7	0.0090	98.59
48 h	11	−0.674	3.329^{-5}	64.20	4.77	−285.9	0.0084	93.77
72 h	11	−0.583	5.329^{-5}	66.00	5.26	−311.9	0.0550	52.91
Blank	11	−0.179	7.329^{-5}	97.21	-	−138.9	-	-

TABLE 4 Electrochemical parameters from EIS equivalent electrical circuits of the specimens.

Parameters	Rs (Ω·cm^2)	Cf (S·sn/cm^2) (n)	Rf (Ω·cm^2)	Cdl (S·sn/cm^2) (n)	Rct (Ω·cm^2)
24 h	971.1	1.86×10^{-8}	6.729×10^5	1.39×10^{-5} (0.574)	2.3×10^{-6}
48 h	955.7	2.77×10^{-8}	5.315×10^5	1.53×10^{-5} (0.309)	1.6×10^{-5}
72 h	908.7	3.57×10^{-9}	4.566×10^4	1.25×10^{-5} (0.354)	8.3×10^{-4}
Blank	10.7	2.42×10^{-9}	775.2	2.41 (0.282)	-

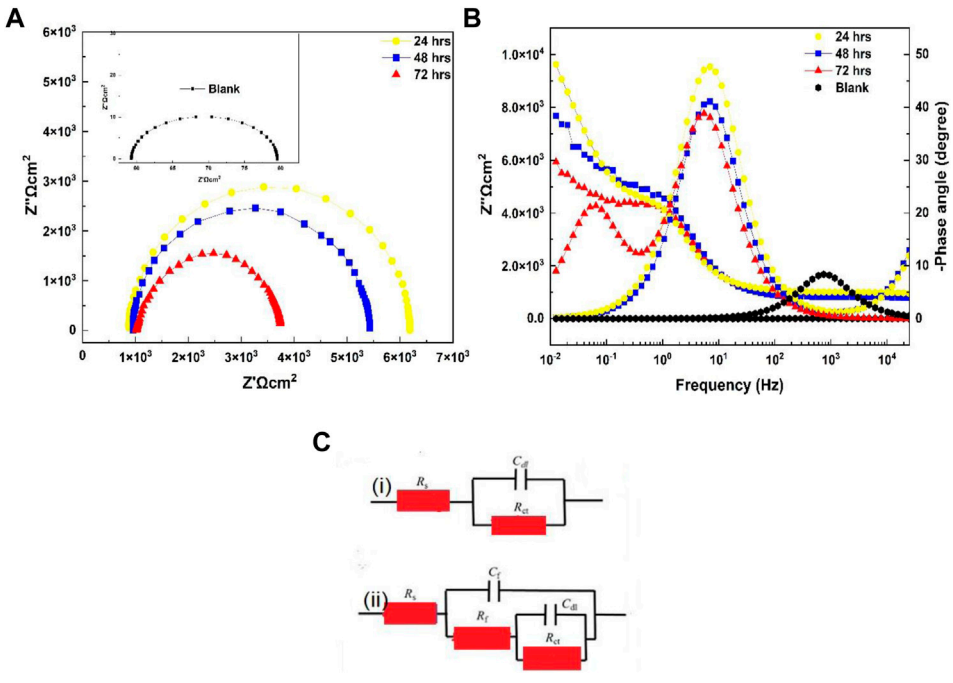

FIGURE 8
Diagram of electrochemical impedance spectroscopy. **(A)** Nyquist plot. **(B)** Bode and phase angle plots of blank aluminum 6101 with coated samples in a 0.001M NaOH solution. **(C)** Equivalent electrical circuits for EIS results: (i) blank aluminum and (ii) coated specimens.

may explain why the cerium conversion coating formed through dip coating was typically Ce (III) with Ce (IV).

3.5 Polarization curves

Figure 7 shows the polarization curves for the untreated and treated specimens. The treated specimens showed higher positive electrochemical corrosion extracted values compared to those of the untreated specimens, showing that the Ce-oxide-based conversion coatings improved corrosion resistance by ennobling the potential and acting as anodic inhibitors. These findings are consistent with the electrochemical corrosive results. The enhancement in potential for specimens coated after treatment at temperatures of 50°C and 70°C was also assessed. Table 3 summarizes the Ecorr, polarization, and EIS data. The I_{corr} was calculated using polarization measurements and EIS data with the RP parameter. The I_{corr} value was significantly improved compared to that of the base material, which was reduced by approximately one order of magnitude. Both specimens had the lowest I-corr values, 0.4 or 0.6 L A cm^2, respectively, which explained the observations of the coating degradation over time in the corrosive alkaline media, less intact, more absorbent, and less adhesive (Xingwen et al., 2001; Valdez et al., 2014).

3.6 Electrochemical impedance spectroscopy

At high-intermediate frequencies, the relaxation method exhibited a phase perspective (h) close to 45, indicating a capacitated behavior with outstanding di-electric characteristics; i.e., the conversion coatings could charge while avoiding the corroding solution's ionic flux (Khan et al., 2022b). In contrast, the untreated 6101 specimen showed an excessive fee >70, indicating lower capacitive features compared to the treated specimens(Figure 8). Furthermore, the phase angle decreased with decreasing frequency, resulting in a second relaxation mode associated with penetration of the 0.001M NaOH solution into the underlying material surface *via* the coating's pores.

Electrochemical analyses were performed under OCP conditions to measure the insulation behavior of the cerium-based coatings. The electrical equivalent circuit (EEC) utilized to characterize the Al alloy 6101 CeCC/NaOH machine significantly affected the interpretation of the EIS data. The fitting technique was carried out using EEC (Figure 8), which consisted of resistance (Rs) representing the ohmic electrolyte resistance, followed by the capacitance of the coating (Cf), another resistance (Rf) representing the coating properties, and a second parallel sub-circuit that associated the interface between the base material and the 0.001M NaOH solution across the porous grid of the coating, double-layer capacitance (Cdl) and charge transfer resistance (Rct) associated with the corrosion operation (Xingwen et al., 2001; Khan et al., 2022b), and a model used for the blank Al alloy 6010 sample showing resistance Rs for the naturally occurring oxide film present on the surface of the substrate, which was rapidly dissolved in the alkaline environment compared to the samples with cerium coatings. The arc-loop of the Nyquist plots decreased over time, with Rct values of 2.3×10^{-6} to 8.3×10^{-4} (Table 4), indicating a large coating adhesion loss in the hard alkaline-conducting solution. Moreover, the presence of the Ce oxide conversion coatings still protected the substrate surface and prevented the alkaline solution from infiltrating between the coating and the substrate surface.

Conclusion

Cerium-based conversion coatings were deposited on Al alloy 6101 after preparation by a dip-coating technique, which was performed four times to attain the desired coating thickness of approximately 25 ± 5 μm. These coatings were mainly cerium-based with good adhesive strength.

1) The coating chiefly contained cerium oxide and presented composite structures, which were ascribed to the repeated dipping process. The XPS results showed that the coating substrate on Al alloy 6101 was mainly protected by Ce (III) and Ce (IV).
2) The cerium-based conversion coating improved the corrosion resistance of the Al alloy 6101 by inhibiting the anodic and cathodic reaction rates in an alkaline environment.
3) Compared to the blank specimen, the cerium-conversion-coated Al alloy 6101 samples showed significantly better corrosion resistance in terms of I_{corr} and polarization resistance (Rp).
4) The eco-friendly conversion coating described in this study demonstrated its promise to replace hazardous chromate coatings. Finally, the conversion treatment significantly increased the corrosion resistance of the Al alloy 6101.

Data availability statement

The original contributions presented in the study are included in the article/Supplementary Materials. Further inquiries can be directed to the corresponding authors.

Author contributions

AK wrote the manuscript and performed all the experiments. H-JZ and ZJ developed the theory and reviewed the manuscript. SE verified the analytical methods. NA and KK interpreted the results. All authors reviewed the results and approved the final version of the manuscript.

Acknowledgments

This research was funded by a Princess Nourah bint Abdulrahman University Research Supporting Project (number PNURSP 2022R19), Princess Nourah bint Abdulrahman University, Riyadh, Saudi Arabia.

Conflict of interest

The authors declare that the research was conducted in the absence of any commercial or financial relationships that could be construed as a potential conflict of interest.

Publisher's note

All claims expressed in this article are solely those of the authors and do not necessarily represent those of their affiliated organizations, or those of the publisher, the editors, and the reviewers. Any product that may be evaluated in this article, or claim that may be made by its manufacturer, is not guaranteed or endorsed by the publisher.

References

Andreeva, R., Stoyanova, E., Tsanev, A., and Stoychev, D. "Influence of the surface pre-treatment of aluminum on the processes of formation of cerium oxides protective films," *Journal of physics: Conference series* 2016, 700, 012049. doi:10.1088/1742-6596/700/1/012049

Campestrini, P., Terryn, H., Hovestad, A., and De Wit, J. (2004). formation of a cerium-based conversion coating on AA2024: Relationship with the microstructure. *Surf. Coatings Technol.* 176 (3), 365–381. doi:10.1016/s0257-8972(03)00743-6

Castano, C. E., O'Keefe, M. J., and Fahrenholtz, W. G. (2015). Cerium-based oxide coatings. *Curr. Opin. Solid State Mater. Sci.* 19 (2), 69–76. doi:10.1016/j.cossms.2014.11.005

Chauhan, L. R., Singh, M., Singh, B., Agarwal, A., Singh, S. K., Bajpai, J., et al. (2022). Development of eco-friendly chemical conversion coating for aluminium substrate. *J. Indian Chem. Soc.* 99 (4), 100392. doi:10.1016/j.jics.2022.100392

Chen, L.-A., Lu, Y.-S., Lin, Y.-T., and Lee, Y.-L. (2021). Preparation and characterization of cerium-based conversion coating on a Fe50Mn30Co10Cr10 dual-phase high-entropy alloy. *Appl. Surf. Sci.* 562, 150200. doi:10.1016/j.apsusc.2021.150200

Chen, S., Zhang, S., Ren, X., Xu, S., and Yin, L. (2015). Cerium-based chemical conversion coating on aluminum alloy to inhibits corrosion in chloride solution. *Int. J. Electrochem. Sci.* 10, 9073–9088.

Eslami, M., Fedel, M., Speranza, G., Deflorian, F., Andersson, N.-E., and Zanella, C. (2017). Study of selective deposition mechanism of cerium-based conversion coating on Rheo-HPDC aluminium-silicon alloys. *Electrochimica Acta* 255, 449–462. doi:10.1016/j.electacta.2017.09.182

Fahrenholtz, W. G., O'Keefe, M. J., Zhou, H., and Grant, J. (2002). Characterization of cerium-based conversion coatings for corrosion protection of aluminum alloys. *Surf. Coatings Technol.* 155 (2-3), 208–213. doi:10.1016/s0257-8972(02)00062-2

Harvey, T. (2013). Cerium-based conversion coatings on aluminium alloys: A process review. *Corros. Eng. Sci. Technol.* 48 (4), 248–269. doi:10.1179/1743278213y.0000000089

Hasannejad, H., Shahrabi, T., Rouhaghdam, A. S., Aliofkhazraei, M., and Saebnoori, E. (2008). Investigation of heat-treatment and pre-treatment on microstructure and electrochemical properties of cerium nano-oxide films on AA7020-T6 by sol–gel methods. *Appl. Surf. Sci.* 254 (18), 5683–5690. doi:10.1016/j.apsusc.2008.03.033

Hinton, B. W., Arnott, D., and Ryan, N. (2003) "The inhibition of aluminium alloy corrosion by cerous cations," *Metals forum*, 7, 211–217.

Hughes, A., Gorman, J., Miller, P., Sexton, B., Paterson, P., and Taylor, R. (2004). Development of cerium based conversion coatings on 2024 T3 Al alloy after rare Earth desmutting. *Surf. Interface Anal.* 36 (4), 290–303. doi:10.1002/sia.1652

Joshi, S., Kulp, E. A., Fahrenholtz, W. G., and O'Keefe, M. J. (2012). Dissolution of cerium from cerium-based conversion coatings on Al 7075-T6 in 0.1 M NaCl solutions. *Corros. Sci.* 60, 290–295. doi:10.1016/j.corsci.2012.03.023

Kamde, M. A., Mahton, Y., Ohodnicki, J., Roy, M., and Saha, P. (2021). Effect of cerium-based conversion coating on corrosion behavior of squeeze cast Mg-4 wt% Y alloy in 0.1 M NaCl solution. *Surf. Coatings Technol.* 421, 127451. doi:10.1016/j.surfcoat.2021.127451

Khan, A. R., Khan, M., Rehman, A. U., Zhao, T. Y., and Zheng, M. (2022a). Novel synthesis and structural investigations of ZnSO4/MgCl2 composite hydrated salt for enhanced thermochemical heat storage applications. *Russ. J. Inorg. Chem.* 67 (7), 1125–1134. doi:10.1134/S0036023622070129

Khan, A. R., Zhao, T., and Zheng, M. (2022b). Composite fabrication of epoxy and graphene oxide coating to enrich the anticorrosion and thermal properties of Carbon-steel. *Surf. Rev. Lett.* 29 (6), 2250072. doi:10.1142/s0218625x2250072x

Khan, A. R., Zheng, M., Cui, Y., and Zhang, H. (2022c). Protection properties of organosilane-epoxy coating on Al alloy 6101 in alkaline solution. *Surf. Engin. Appl. Electrochem.* 58 (3), 281–289. doi:10.3103/s1068375522030036

Khast, F., Saybani, M., and Dariani, A. A. S. (2022). Effects of copper and manganese cations on cerium-based conversion coating on galvanized steel: Corrosion resistance and microstructure characterizations. *J. Rare Earths* 40 (6), 1002–1006. doi:10.1016/j.jre.2021.07.015

Kiyota, S., Valdez, B., Stoytcheva, M., Zlatev, R., and Bastidas, J. M. (2011). Anticorrosion behavior of conversion coatings obtained from unbuffered cerium salts solutions on AA6061-T6. *J. Rare Earths* 29 (10), 961–968. doi:10.1016/s1002-0721(10)60579-0

Kulinich, S., Farzaneh, M., and Du, X. (2007). Growth of corrosion-resistant manganese oxide coatings on an aluminum alloy. *Inorg. Mat.* 43 (9), 956–963. doi:10.1134/s0020168507090087

Li, F. M., Huang, L., Zaman, S., Guo, W., Liu, H., Guo, X., et al. (2022). Corrosion Chemistry of electrocatalysts. *Advanced Materials*. 25:e2200840. doi:10.1002/adma.202200840

Li, L., Desouza, A. L., and Swain, G. M. (2013). *In situ* pH measurement during the formation of conversion coatings on an aluminum alloy (AA2024). *Analyst* 138 (15), 4398–4402. doi:10.1039/c3an00663h

Mohammadloo, H. E., Sarabi, A., Hosseini, R. M., Sarayloo, M., Sameie, H., and Salimi, R. (2014). A comprehensive study of the green hexafluorozirconic acid-based conversion coating. *Prog. Org. Coatings* 77 (2), 322–330. doi:10.1016/j.porgcoat.2013.10.006

Pardo, A., Merino, M., Arrabal, R., Viejo, F., and Munoz, J. (2007). Ce conversion and electrolysis surface treatments applied to A3xx. x alloys and A3xx. x/SiCp composites. *Appl. Surf. Sci.* 253 (6), 3334–3344. doi:10.1016/j.apsusc.2006.07.028

Paussa, L., Andreatta, F., Navarro, N. R., Durán, A., and Fedrizzi, L. (2012). Study of the effect of cerium nitrate on AA2024-T3 by means of electrochemical micro-cell technique. *Electrochimica Acta* 70, 25–33. doi:10.1016/j.electacta.2012.02.099

Sainis, S., and Zanella, C. (2022). A localized study on the influence of surface preparation on the reactivity of cast Al-7Si-1Fe and Al-7Si-2Cu-1Fe alloys and their effect on cerium conversion coating deposition. *Appl. Surf. Sci.* 585, 152730. doi:10.1016/j.apsusc.2022.152730

Scholes, F., Soste, C., Hughes, A., Hardin, S., and Curtis, P. (2006). The role of hydrogen peroxide in the deposition of cerium-based conversion coatings. *Appl. Surf. Sci.* 253 (4), 1770–1780. doi:10.1016/j.apsusc.2006.03.010

Sharif, H. M. A., Ali, M., Mahmood, A., Asif, M. B., Din, M. A. U., Sillanpää, M., et al. (2022). Separation of Fe from wastewater and its use for NOx reduction; a sustainable approach for environmental remediation. *Chemosphere* 303, 135103. doi:10.1016/j.chemosphere.2022.135103

Sharif, H. M. A., Asif, M. B., Wang, Y., Hou, Y.-N., Yang, B., Xiao, X., et al. (2023). Spontaneous intra-electron transfer within rGO@ Fe2O3-MnO catalyst promotes long-term NOx reduction at ambient conditions. *J. Hazard. Mater.* 441, 129951. doi:10.1016/j.jhazmat.2022.129951

Tang, J., Han, Z., Zuo, Y., and Tang, Y. (2011). A corrosion resistant cerium oxide based coating on aluminum alloy 2024 prepared by brush plating. *Appl. Surf. Sci.* 257 (7), 2806–2812. doi:10.1016/j.apsusc.2010.10.065

Valdez, B., Kiyota, S., Stoytcheva, M., Zlatev, R., and Bastidas, J. (2014). Cerium-based conversion coatings to improve the corrosion resistance of aluminium alloy 6061-T6. *Corros. Sci.* 87, 141–149. doi:10.1016/j.corsci.2014.06.023

Xingwen, Y., Chunan, C., Zhiming, Y., Derui, Z., and Zhongda, Y. (2001). Study of double layer rare Earth metal conversion coating on aluminum alloy LY12. *Corros. Sci.* 43 (7), 1283–1294. doi:10.1016/s0010-938x(00)00141-4

Zaman, S., Huang, L., Douka, A. I., Yang, H., You, B., and Xia, B. Y. (2021). Oxygen reduction electrocatalysts toward practical fuel cells: Progress and perspectives. *Angew. Chem. Int. Ed. Engl.* 133 (33), 17976–17996. doi:10.1002/ange.202016977

Zaman, S., Su, Y. Q., Dong, C. L., Qi, R., Huang, L., Qin, Y., et al. (2022a). Scalable molten salt synthesis of platinum alloys planted in metal–nitrogen–graphene for efficient oxygen reduction. *Angew. Chem. Int. Ed. Engl.* 134 (6), e202115835. doi:10.1002/anie.202115835

Zaman, S., Wang, M., Liu, H., Sun, F., Yu, Y., Shui, J., et al. (2022b). Carbon-based catalyst supports for oxygen reduction in proton-exchange membrane fuel cells. *Trends Chem.* 4, 886–906. doi:10.1016/j.trechm.2022.07.007